Study of Spectrum Analysis and Signal Biasing for Dielectric Barrier Discharge Actuator

Pengfei Zhao[a] and Subrata Roy[b]
Applied Physics Research Group, Department of Mechanical and Aerospace Engineering
University of Florida, Gainesville, FL 32611-6300, USA

This paper presents experiments for understanding the dielectric barrier discharge actuators. Two aspects concerning the actuator are investigated in this work. The first one is a study on the characteristics of plasma spectrum which were obtained by an optical emission system. Results from optical emission spectra show that there are two active regions in one cycle, the profiles of which are different for different applied voltages. The second aspect of the paper investigates how the force generated by the actuator varies under biased voltage signals. The increase of force is reported for increasing negative biases. These results can provide an insight into how negative ions play a dominant role in force generation.

Nomenclature

ε_r = relative dielectric constant of the dielectric material
w = width of the exposed electrode (mm)
l = length of the exposed electrode (cm)
t_e = thickness of the copper electrodes (mm)
t_d = thickness of the dielectric material (mm)
f = focal length of the lens (mm)
T_{vib} = vibrational temperature (K)
I_{ij} = emission intensity between level *i* and level *j*
A_{ij} = Einstein coefficient for spontaneous electron-vibrational transition from level *i* to level *j*
N_i = concentration of $N_2(C^3\Pi_u, i)$
n_k = concentration of $N_2(X^1\Sigma_g^+, k)$
q_{ik} = Frank-Condon factor
E_k = vibrational energy of $N_2(X^1\Sigma_g^+, k)$
γ^2 = square of correlation coefficients
k_s = slope of the fitting line (mN/(m•kV))
F_{obs} = observation for F-test
F = force generated by the actuator (N)
q_n = net charge of the plasma (C)
E = electric field in the plasma (V/m)
F_b = force generated by the biased signal (N)
E_o = original electric field (V/m)
E_b = electric field from the offset (V/m)

I. Introduction

THE dielectric barrier discharge (DBD) plasma actuator is becoming a popular device for active flow control. Because it has no mechanical moving parts, the DBD plasma actuators are of high reliability and easy to accommodate on any other components at any location. Specifically, the lifetime of this device is expected to be much longer than mechanical reciprocal devices such as synthetic jet actuator. In mid 1990s, Roth et al.[1,2] first reported that induced electro-hydrodynamic (EHD) body force can be generated using these actuators to manipulate the low velocity boundary layer over a flat plate. Since then these actuators have been tested as flow control devices

[a] Graduate Student, Student Member AIAA, tramperfa@ufl.edu
[b] Associate Professor, Associate Fellow AIAA, roy@ufl.edu

on stationary[3-5] and oscillating airfoils[6], active noise control[7,8], low pressure turbine blades[9,10] and bluff bodies[11]. As continued progress is made in the DBD actuator design, there is no doubt that new applications will continue to emerge.

The DBD plasma actuator typically only consists of two electrodes placed asymmetrically on the two sides of a dielectric board, one electrode is exposed to ambient air and the other one is enclosed to prevent discharge from occurring on the lower surface. The exposed electrode is powered with a radio frequency (RF) high voltage signal, while the enclosed electrode is grounded. A reverse powering scheme is also practical.

Over the past couple of decades, input parameters of these actuators, like driving voltage, frequency, geometric design, signal waveforms and various other aspects, have been investigated extensively to understand the relative importance of each parameter[12-15]. However, adding bias to the input waveform is a unique way to investigate the kind of particles, positive or negative ions, which have majority contribution in generating the EHD force. In this paper, we introduce biasing as the tool to probe into the dynamics of the force generation mechanism.

Also, spectrum analysis is used to investigate the plasma generated by the actuator. From the spectrum of plasmas, one can get temperature, intensity, species, etc[16]. Spectrum intensity indicates the density of a certain species. Vibrational temperature of the particles in plasma is one major parameter in energy transformation process of the actuator. So, the spectrum is a powerful tool in studying the DBD plasma actuator.

This paper contains two parts. The first part presents a study of the characteristics of spectrum obtained from the actuator. The goal is relating these characteristics to voltage and current signals. The second part mainly focuses on the force measurements with positive and negative voltage biases. The contribution of positive and negative ionized particles to the force generation process by the actuator is discussed.

II. Experiment Setup

A. DBD Plasma Actuator

A standard linear DBD plasma actuator is used in this experiment. It consists of two copper electrodes and one piece of dielectric board made of acrylic; one electrode is exposed in the ambient air and the other one is encapsulated by multi-layer electric insulating tape to ensure no discharge occurs on the lower surface of the dielectric board. These two electrodes were placed asymmetrically on the two sides of the dielectric board with no inner gap in horizontal x-direction shown in figure 1a. Both electrodes were made of copper tape with the thickness, t_e, of 0.07 mm, and the thickness, t_d, of the acrylic board between these electrodes is 1.87mm with a relative dielectric constant, ε_r, of 3. The width, w, of the upper electrode is 5 mm, while the lower electrode's width is, $4w$, 20 mm. Both electrodes have a length, l, of 8 cm. The actuator depicted in figure 1b shows the detailed dimensions of the dielectric board used in the experiment which also affect the performance of the actuator.

In order to ionize the ambient air, a high voltage RF signal was supplied on the exposed electrode, while the encapsulated electrode was grounded. A sinusoidal wave was generated by an arbitrary waveform generator (Tektronix AFG3022B). The input signal was further amplified by a high voltage amplifier. With proper signal, plasma was generated at the edge of exposed electrode and extended to the top of the encapsulated electrode. Two voltages, $16kV_{pp}$ and $20kV_{pp}$, were investigated in this study.

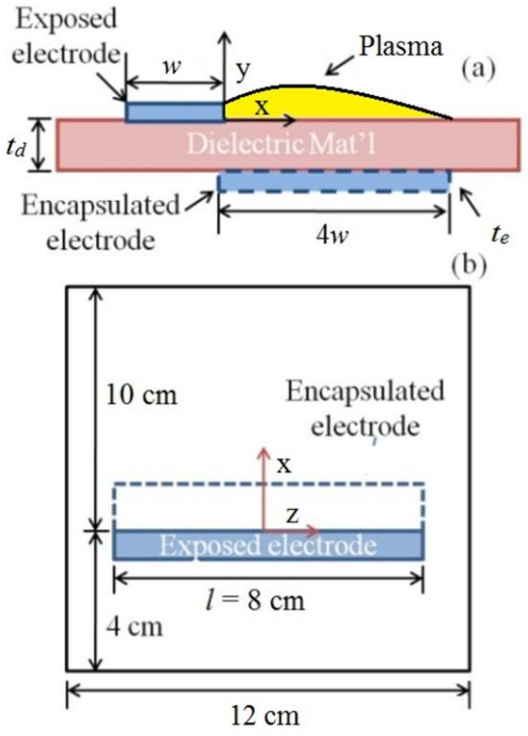

Figure 1. Schematic of DBD plasma actuator: (a) side view and (b) top view. From Durscher and Roy, 2011, used with permission.

B. Optical Measurement

Optical Emission System (OES) was also used in this work due to the advantage of non-intrusive measurement.

Figure 2 shows the optical setup of the experiment. This is a typical optical system for OES technique which consists of lens with tube, optical fiber connected to spectrometer and optical chopper placed in front of the fiber probe. The DBD plasma actuator was mounted vertically on a three-dimensional translating stage which can easily adjust the position of the actuator. The chopper, lens and optical fiber were located on a rail system to ensure the light path is straight. We used a 1-inch diameter THORLABS uncoated UV fused silica bi-convex lens with the focal length, *f*, of 35 mm, which has good performance at a wavelength range from 180 nm to 2100 nm. The Optical fiber and the plasma actuator were located at the 2*f* plane on each side of the lens, which ensures that the images obtained through the optical fiber were of the same size as plasma actuator. The focus point of the lens was located at the middle of the exposed electrode in z-direction and at the strongest point in x-direction (Figure 2). The spectrometer (Ocean Optics USB 2000+), which can obtain spectra from the wavelength range of 180 nm – 850 nm, was also employed to obtain the real-time spectra. Furthermore, the experiment was housed within a ventilated box, and a piece of black paper was located behind the DBD plasma actuator to reduce the background lighting influence.

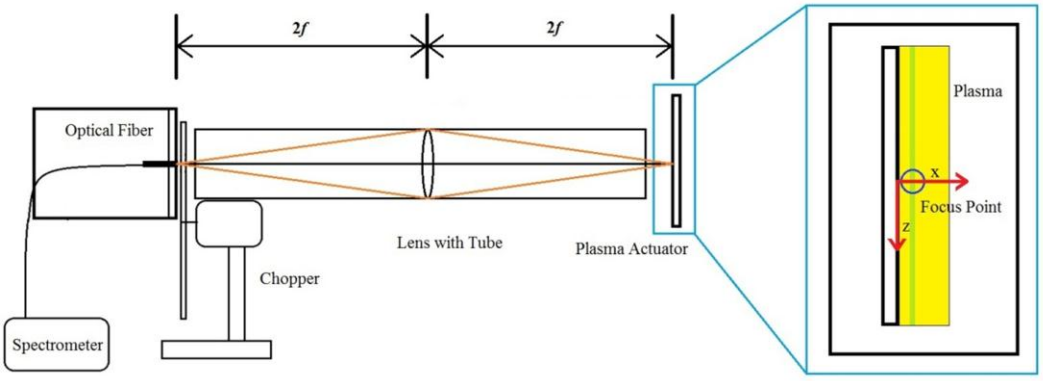

Figure 2. System for optical measurement.

The optical chopper we used is THORLABS MC2000 which has a 50% duty ratio originally (Figure 3a). After attaching chopper shelter on each vane shown in figure 3b, we got a 10% duty ratio chopper which means this one can give us a better time resolution. Phase-lock function which can help us obtain light from an exact phase of the cycle is also available on the chopper used in this work.

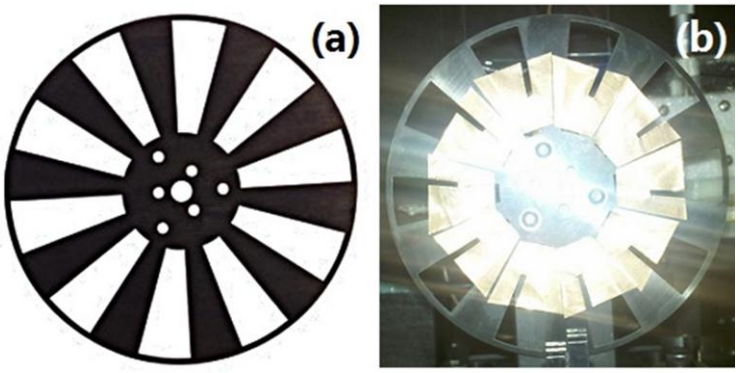

Figure 3. Chopper: (a) original (b) after remodeling.

According to this work, spectrum was measured at the edge of the exposed electrode where we can obtain the maximum intensity. The major spectra come from the second positive system (SPS) of transition $N_2(C^3\Pi_u \rightarrow B^3\Pi_g)$. No spectra from oxygen and nitrogen oxide were observed within the wavelength range. The vibrational temperatures (T_{vib}) were calculated from fitting experiment results with simulated results generated by Specair (version 2.2.0.0, figure 4), which can calculate spectra simulation for various gas particles and transition of various conditions. The electron temperature, rotational temperature and vibrational temperature are three main parameters when fitting with simulated data. However, since our plasma is low

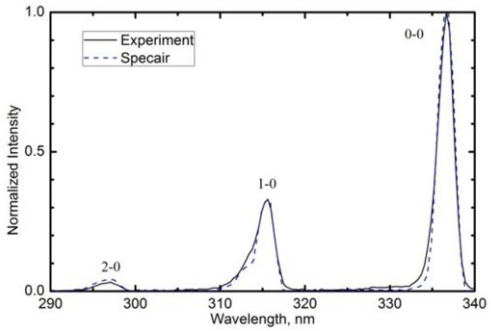

Figure 4. Spectrum fitting with simulation

temperature plasma, the vibrational temperature has dominant effect on the spectra obtained during experiments.

The SPS is a well-studied spectrum system of N_2. Let us consider SPS emitted under the transition $N_2(C^3\Pi_u, i \rightarrow B^3\Pi_g, j)$ with the emission intensity in equation 1, where i and j are the vibrational energy levels. The concentration of N_i is calculated from equation 2, where k is the vibrational energy level of the $N_2(X^1\Sigma_g^+)$. Since we also have a Boltzmann distribution of the $N_2(X^1\Sigma_g^+, k)$ molecules on vibrational energy level in equation 3, we can combine equation 1-3 to get equation 4 which shows that vibrational temperature can be determined only on I_{00}/I_{10}. So, our fitting strategy only depended on the intensity ratio between 0-0 peak and 1-0 peak shown in figure 4.

$$I_{ij} = A_{ij}N_i \tag{1}$$

$$\mathrm{N}_i = \sum_k n_k q_{ik} \tag{2}$$

$$n_k = n_0 exp(-E_k/T_{vib}) \tag{3}$$

$$\frac{I_{00}}{I_{10}} = \frac{A_{00}}{A_{10}} \frac{\sum_k exp(-E_k/T_{vib}) q_{0k}}{\sum_k exp(-E_k/T_{vib}) q_{1k}} \tag{4}$$

C. Force Measurement

Force measurement system mainly depends on our group's previous work[17], which shows a good agreement with control volume method. Force measurements were obtained using an Ohaus precision balance (Adventurer™ Pro AV313C). The actuators were mounted on an acrylic stand which located on the center of the balance. The acrylic stand also protruded through a small opening in a Faraday's cage, which was used to shield the balance from any electromagnetic interference due to the high alternating electric fields required to generate the plasma discharge. To prevent ambient room flow from influencing the sensitive scale with resolution of 1 mg, the entire setup was housed in a large quiescent chamber with dimensions 61 cm x 61 cm x 82 cm (width x depth x height). However chamber was slightly vented, small amounts of ozone (an unavoidable product of the discharging process) spilled out into the laboratory air which is harmless due to the small scale of leakage. And the level of ozone in the room is continuously monitored by an Aeroqual SM-70 ozone monitor during experiment running. In order to reduce the rigidity of the wire from influencing the reading, thin insulated wires (34 AWG) were used to connect the high-voltage input signal and ground to the actuator. Between every two input signals measured, there was 2 minutes for the system to reach a stable condition for measure. And for each input signal, 10 measurements were recorded from the scale with a 10s interval. The uncertainty associated with the given force measurement is below 5% (at 95% confidence).

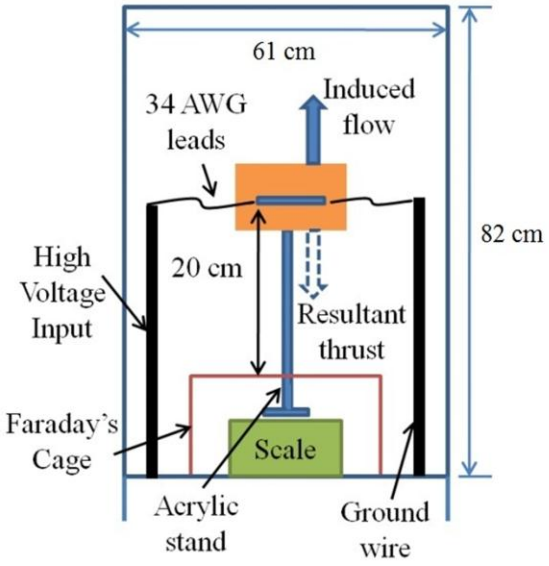

Figure 5. Force measurement system. From Durscher and Roy, 2011, used with permission.

III. Results

The following section contains two related parts. Part A describes the spectrum analysis with different input signals. And Part B presents the study on force measurement of the actuator with different offsets which can give us physical insight of the electro-hydrodynamic (EHD) body force generation mechanism.

A. Spectrum Study

1. Typical Actuator Spectrum

Figure 6 shows the typical peak intensity at 337.13 nm (0-0) and vibrational temperature for SPS of the transition $N_2(C^3\Pi_u \rightarrow B^3\Pi_g)$, along with voltage and current signal synchronously in two cycles. Since we encapsulated the grounded electrode with multi-layer electric insulating tape, only the positive-going slope of sine wave has large current spikes (green line) in the voltage and current curve (Figure 6a), which represents strong ionization process. The intensity curve (Figure 6c) shows only two peaks in one cycle, and these two peaks appear exactly at positive-going slope and negative-going slope of the voltage signal. This characteristic implies that the discharging process only occurs at the slope of the signal, and that the discharge mainly depends on the slope of the input signal. Furthermore, vibrational temperature can only be fitted well with simulation results from Specair during these two peaks since the spectrum in other part of the cycle is too small to be used for fitting. Figure 6b shows that the vibrational temperature, T_{vib}, at the positive-going slope of the cycle (~3400K) is higher than that of the negative-going slope by about 1000K. However, according to the full width at half maximum (FWHM) of intensity, the positive-going slope has a wider FWHW than that of the negative-going slope, which indicates the durations of discharge processes at the two slopes are different.

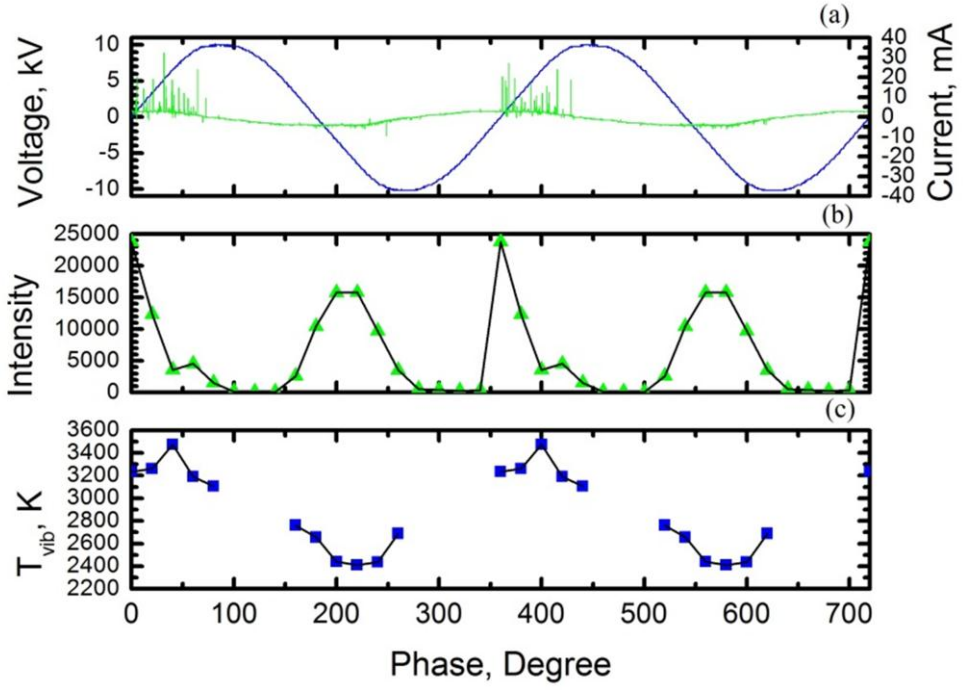

Figure 6. Comparison of the (a) voltage & current curve, (b) vibrational temperature and (c) intensity cure get from the spectrum of plasma.

2. Spectra analysis with different voltage

Figure 7 shows the spectra analysis for two cases: case 1 is powered by a signal with a peak-to-peak voltage of 16 kV, and case 2 is supplied by a 20 kV peak-to-peak waveform. Both cases have the same driving frequency of 1 kHz, which is limited due to the chopper we used. Both intensity (Figure 7a) and vibrational temperature (Figure 7b) show only slight differences between two cases at the negative-going slope, while relatively large changes occurred at the positive-going slope. This phenomenon indicates that when voltage changes, the negative-going slope is more stable than the positive-going slope. Combine the result above, the discharge processes at these two slopes have different duration and different responds to voltage changing. So, we can conclude here the discharge processes during the negative-going and positive-going slopes are different. Similar result was also reported by Enloe et al.[18].

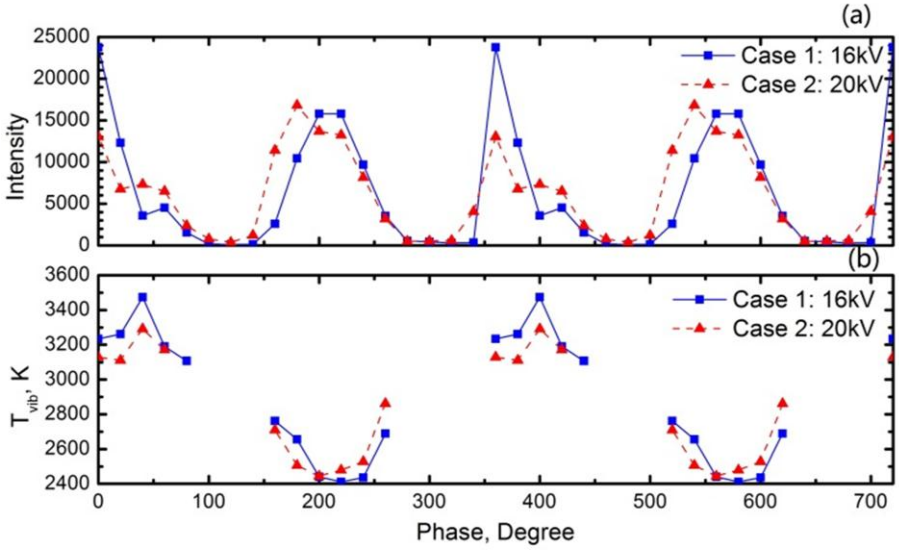

Figure 7. Spectrum analysis: (a) intensity (b) T_{vib}.

B. Biased Signal Study

1. Input Signal

In order to evaluate the effect of the offset that added to the input signal, the biased input signal is defined in this part. As shown in Figure 8, for a 16kV peak-to-peak input sine waveform, a -8 kV (negative) offset means whole signal should below ground, while a +8 kV (positive) bias should be all above ground potential.

Since the discharge process depends mainly on the temporal slope of the input signal, the basic assumption for biasing study is that the discharge process only relies on the shape of the waveform. We can further assume that the ionization and excitation process remains the same with different offsets. Then offset is the only factor that affects force measurements in our experiment.

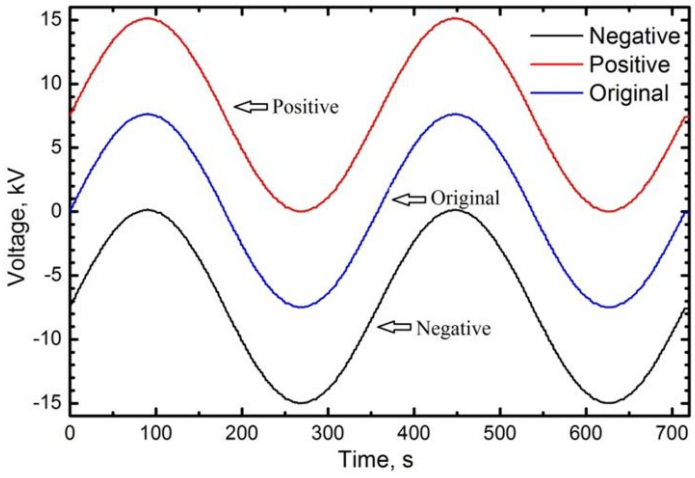

Figure 8. Input voltage signals

2. Spectra analysis with offsets

The results shown in Figure 9 indicate that intensity and T_{vib} were nearly identical regardless of bias variation. In this case, we calculate the square of correlation coefficient for these data. For positive-going slope, the squares of correlation coefficients, γ^2, are 0.056 and 0.050 for intensity and T_{vib}, respectively. For negative-going slope, the squares of correlation coefficients are 0.139 and 0.0001, respectively. A statistical test was also conducted and

analysis of variance (ANOVA) showed all four data groups have no correlation with offsets at 95% confidence level. These data imply the discharge process is relatively stable during offset changing. These data support the assumption that biased signals have the same discharge like the standard signal.

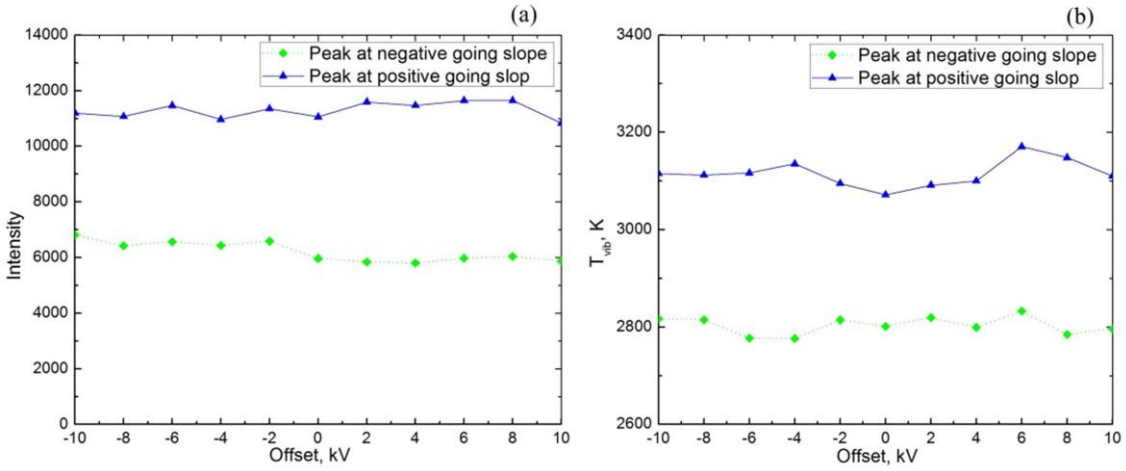

Figure 9. (a) Intensity and (b) T_{vib} at different offset

3. Force Measurement

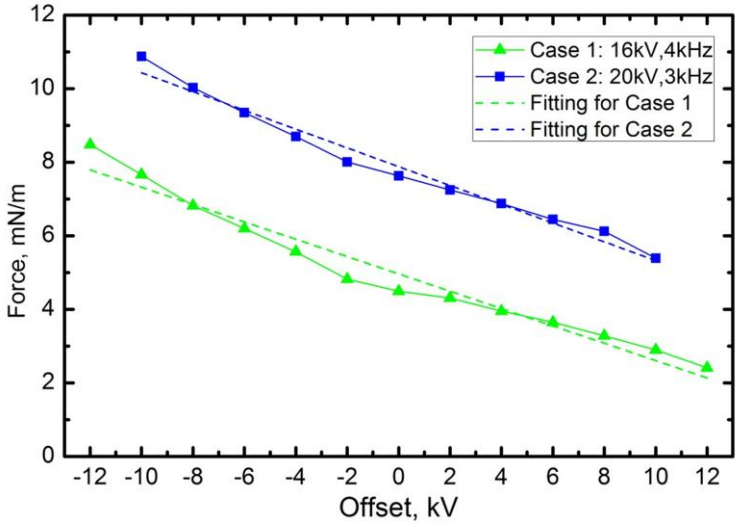

Figure 10. Force measurements vs. offset.

In order to study the effect of bias on force generation, two cases of different voltages were measured. The same actuator was used throughout these two cases. Case 1 used a signal of 16 kV peak-to-peak voltage with 3 kHz frequency and the range of bias is from -12 kV to 12 kV. Case 2 was operated with a signal of 20 kV peak-to-peak voltage, 4 kHz frequency, and the offset range is -10 kV to 10 kV. The frequency is different for keeping the same amount of energy consumed in these two cases. The results of this study, presented in Figure 10, indicate that there is a decrease in thrust as bias is increased from negative to positive. This decrease is independent of two cases investigated. Statistical tests were also conducted for these results. The squares of correlation coefficient are 0.960 and 0.966 for case 1 and case 2, which means that there is a strong linear relationship between force generated by plasma actuator and the offsets added to the signal.

To quantify this linear relationship between force and offsets, we obtained the slopes, *k*, of the fitting lines shown in table 1. ANOVA was also conducted for this part and the F-test results are also shown in table 1. The slopes of two cases are in same order and larger voltage has higher slope, which is reasonable since case 2 can generate more force without bias. From the statistical results for the value of k_s, one can also find strong evidence for the accuracy of the results.

Case	F_{obs}	P-value for F_{obs}	k_s, mN/(m•kV)	P-value for k_s
1: 16kV, 4kHz	334.32	2.87E-20	-0.226	7.32E-21
2: 20kV, 3kHz	325.40	1.35E-17	-0.256	3.55E-17

Table 1. Statistical analysis for force measurement

The force measured by the precision balance is mainly generated from momentum transported from the net charge of the plasma which is accelerated by the electric filed in x-direction. So, the key parameters that can affect the force generation are only net charge densities and electric field. The relationship between force, F, net charge, q_n, and electric field, E, is shown in equation 5a. After the signal is biased, the relationship is become equation 5b.

$$F = q_n E \tag{5a}$$

$$F_b = q_n(E_o + E_b) \tag{5b}$$

According to our previous assumption, the discharge process only depends on the waveform of the input signal which indicates the discharge process remains the same while the offset changes. So, we infer that the net charge, as a result of the discharge process, does not change while the offset changes. Then, the force only depends on the electric field which consists of a constant original electric flied, E_o, and a electric field from the offset, E_b. And the biased electric field, E_b, is in direct proportion to the offset added on the input signal. As we can see from the force measurements, force decreases during the offset increases with a good linear relationship. So combining all conditions listed above, the only reasonable inference is that the net charge is negative. Furthermore, since electrons easily drift away in the electric field due to much smaller inertia. The net charge in electric field mainly consists of positive and negative ions. So we can conclude that negative ions are the main active particles in force generation form this study.

IV. Conclusion

Time resolutions of spectra of plasma actuator for different voltages were investigated using an optical system. In the whole cycle investigated, two intensity peaks were observed at the slopes of the input waveform. And the different vibrational temperatures were also founded at these slopes. With further study on spectra, we found that the discharging processes at two peaks are different and the negative-going slope is the one with better stability. According to the data obtained, we can also conclude that discharges at two slopes have different processes.

The system response has been tested with respect to a series of input sine wave signals with different offsets. From the spectrum captured, the main parameters showed no significant difference among different biases added, which gives us confidence to assume the plasma generated by signals with different biases added have similar properties. Then the force generated by these signals was investigated. The results indicate that there is a decrease when the offset is increased, which means one can generate larger force with negative bias. It is a strong evidence to validate that negative ions play a more important role than positive ions in force generation.

References

[1]Roth, J. R., Sherman, D. M., and Wilkinson, S., "Boundary layer flow control with one atmosphere uniform glow discharge surface plasma," *36th AIAA Aerospace Science Meeting*, AIAA Paper 1998-0328, Reno, NV, 1998,

[2]Roth, J. R., Sherman, D. M., and Wilkinson, S. P., "Electrohydrodynamic flow control with a glow-discharge surface plasma," *AIAA Journal*, Vol. 38, 2000, pp. 1166–72,

[3]He, C., Corke, T., and Patel, M., "Plasma flaps and Slats: An Application of Weakly Ionized Plasma Actuators," *Journal of Aircraft* , Vol. 46, No. 3, 2009, pp. 864-73,

[4]Benard, N., Braud P., Jolibois, J., and Moreau, E., "Airflow Reattachment Along a NACA 0015 Airfoil by Surfaces Dielectric Barrier Discharge Actuator - Time Resolved Particle Image Velocimetry Investigation," *4th Flow Control Conference*, AIAA Paper 2008-4202, Seattle, WA, June 2008,

[5]Visbal, M. R., Gaitonde, D. V., and Roy, S., "Control of Transitional and Turbulent Flows Using Plasma-Based Actuators," *AIAA Fluid Dynamics Conference and Exhibit*, AIAA Paper 2006-3230, San Francisco, CA, June, 2006,

[6]Post, M. and Corke, T., "Separation Control Using Plasma Actuators: Dynamic Stall Vortex Control on Oscillating Airfoil," *AIAA Journal*, Vol. 44, No. 12, 2006, pp. 3125-35,

[7]Thomas, F. O., Kozlov, A., and Corke, T. C., "Plasma Actuators for Landing Gear Noise Reduction," *11th AIAA/CEAS Aeroacoustics Conference (26th AIAA Aeroacoustics Conference)*, AIAA Paper 2005-3010, Monterey, CA, May, 2005,

[8]Li, Y., Zhang, X., and Huang, X., "The use of plasma actuators for bluff body broadband noise control," *Experiments in Fluids*, No. 11, 2010,

[9]Huang, J., Corke, T. C., and Thomas, F. O., "Plasma Actuators for Separation Control of Low-Pressure Turbine Blades," *AIAA Journal*, Vol. 44, No. 1, 2006, pp. 51- 57,

[10]Rizzetta, D. P., and Visbal, M. R., "Plasma-Based Flow-Control Strategies for Transitional Highly Loaded Low-Pressure Turbines," *J. Fluids Eng*., Vol. 130, Issue 4, 2008,

[11]Sung, Y., Kim, W., Mungal, M. G., and Cappeli, M., "Aerodynamic Modification of Flow over Bluff Objects by Plasma Actuation," *Experiments in Fluids*, Vol. 41, No. 3, Sept. 2006, pp. 479–486,

[12]Abe, T., Takizawa, Y., Sato,S., and Kimura, N., "A Parametric Experimental Study for Momentum Transfer by Plasma Actuator," *45th AIAA Aerospace Sciences Meeting and Exhibit*, AIAA Paper 2007-187, Reno, NV, January, 2007,

[13]Roth, J. R., and Dai, X., "Optimization of the Aerodynamic Plasma Actuator as an Electrohydrodynamic (EHD) Electrical Device," *44th AIAA Aerospace Sciences Meeting and Exhibit*, AIAA Paper 2006-1203, Reno, NV, January, 2006,

[14]Enloe, C. L., McLaughlin, T. E., Van Dyken, R. D., Kachner, K. D., Jumper, E. J., Corke, T. C., Post, M., and Haddad, O., "Mechanisms and Responses of a Single Dielectric Barrier Plasma Actuator: Plasma Morphology," *AIAA Journal*, Vol. 42, No. 3, 2004, pp 589-594,

[15]Enloe, C. L., McLaughlin, T. E., Van Dyken, R. D., Kachner, K. D., Jumper, E. J., Corke, T. C., Post, M., and Haddad, O., "Mechanisms and Responses of a Single Dielectric Barrier Plasma Actuator: Geometric Effects," *AIAA Journal*, Vol. 42, No. 3, 2004, pp 595- 604,

[16]Stanfield S. A., and Menart J., "Vibrational temperatures and relative concentration of $N_2(C_3\Pi_u)$ and $N_2{}^+(B_2\Sigma_u)$ for an asymmetric surface mode dielectric barrier discharge," *47th AIAA Aerospace Sciences Meeting and Exhibit*, AIAA Paper 2009-653, Orlando, FL, January, 2009,

[17]Durscher, R., and Roy, S., "Force Measurement Techniques and Preliminary Results Using Aerogels and Ferroelectrics for Dielectric Barrier Discharge Actuators," *42nd AIAA Plasmadynamics and Lasers Conference*, AIAA Paper 2011-3735, Honolulu, HI, June, 2011,

[18]Enloe, C. L., McHarg, M. G., and McLaughlin T. E., "Time-correlated force production measurements of the dielectric barrier discharge plasma aerodynamic actuator," *Journal of Applied Physics*, 103, 073302 (2008).